Adaptive Unstructured Grid Generation for Viscous Flow Applications

David L. Marcum*
Mississippi State University,
Mississippi State, Mississippi 39762

Introduction

UNSTRUCTURED grid technology provides a powerful capability for computing complex flowfields about realistic aerospace configurations. The geometric flexibility of the unstructured approach makes it ideally suited for geometrically complex configurations and, when combined with solution adaptation, for complex physics. The full potential of this approach, for many applications, can only be realized when it is truly capable of handling complex geometries and adapting to complex physics in an automatic and efficient manner. Several unstructured grid generation and flow solver procedures with and without solution adaptation have been developed and successfully demonstrated for inviscid flow about realistic configurations. However, for viscous flowfields, considerably less work has been done,[1–4] especially in the area of solution adaptation. Further improvements in efficiency, robustness, and grid quality of the solution adaptation and grid generation procedures are needed for viscous flow applications.

The objective of this work is to develop a procedure for efficient generation of high-quality solution-adapted grids suitable for viscous flow applications. The overall approach taken in this work for solution adaptation is to generate high-aspect-ratio elements in the boundary-layer regions and to capture inviscid features and detached viscous features independently using different adaptation procedures.

Unstructured Grid Generation Procedure

The triangular/tetrahedral grid generation procedure used in the present work is a combination of automatic point creation, advancing-normal point placement, advancing-front point placement, and connectivity optimization schemes.[5,6] A valid grid is maintained throughout the grid generation process. Points are generated using either advancing-front type placement for isotropic elements or advancing-normal type point placement for high-aspect-ratio elements. The connectivity for new points is initially obtained from direct subdivision and then improved by iteratively using local reconnection subject to a quality criterion. A min-max type (minimize the maximum angle) criterion is used. The overall procedure is applied repetitively until a complete field grid is obtained. High-quality isotropic and high-aspect-ratio element two- and three-dimensional grids have been efficiently generated about geometrically complex configurations using this procedure.[5,6]

Solution Adaptation

The previously described grid generation procedure generates a field grid with point spacing based on the boundary point spacing. The procedure can be modified to allow the field spacing to vary based on a computed flowfield solution. Solution adaptation for inviscid features is implemented in the present procedure using an adaptation source approach.[7] In this approach, the flowfield is reduced to a set of points located in regions where there are features of interest, e.g., shock waves, rapid expansions, stagnation points, contact discontinuities, etc. A split feature detector[7] is used to isolate features of different types and varying magnitude. At each identified point, an adaptation source is created with an associated desired element size that is proportional to the solution gradients. Within the standard grid generation procedure the function that controls element size is modified by the adaptation sources and their associated desired element size. Each adaptation source modifies the function for all existing grid points that are within a radius of influence. The radius of influence is based on the existing local element size. This procedure can efficiently produce a very smooth and focused adaptation. Further details are presented in Refs. 7 and 8.

For viscous flowfields, the boundary-layer regions are in general known a priori and require solution adaptation only to obtain an appropriate normal spacing at the surface. Location and strength of field features such as wakes are not usually known a priori. Solution adaptation of these features is required to provide reasonable resolution. The overall approach taken in this work is to generate high-aspect-ratio elements in the boundary-layer regions and capture inviscid features and detached viscous features using solution adaptation. The adaptation source approach can be extended to provide adaptation for detached viscous features. However, it is difficult to isolate boundary-layer and field viscous features. An alternative approach is considered here wherein boundary-layer regions, detached viscous regions, and inviscid features are each treated separately.

The approach used for viscous adaptation is to track selected streamlines, create sets of streamline points, and resolve the grid in the vicinity of the streamline points. Starting with an initial solution, streamlines are generated from areas near boundary surface discontinuities. The individual streamlines can be treated as new boundary surfaces embedded within the field. A desired point distribution is then generated along each streamline for subsequent grid regeneration. These points can be treated in multiple ways within the grid generation process. They can be treated as adaptation sources for isotropic refinement or as sets of points on embedded boundary surfaces. A triangulation of boundary points for a double strut application with embedded streamline boundaries and field adaptation sources is shown in Fig. 1. The embedded boundaries provide a natural framework for directional refinement and automatic alignment with the wake. In comparison to isotropic refinement, directional refinement requires far fewer points and consequently less flow solver CPU time and memory to resolve a flowfield to the same level. To maintain element quality, directional refinement with even moderately high-aspect-ratio elements requires precise control of point placement. The precise control can readily be provided by advancing from an embedded boundary and generating the points using advancing-normal point placement. This also provides a natural alignment of the elements with the embedded boundary, which in the present application represents a physical feature. For two-dimensional applications use of isotropic elements, although not optimal, is not unreasonable as memory requirements are not as severe as they are in three dimensions.

In the overall procedure, an initial grid is generated with high-aspect-ratio elements adjacent to the boundary surfaces. The initial grid spacing must be sufficient to capture the boundary-layer and near surface features. Initial resolution of these features is only required to a level such that they can be detected. A flowfield solution is then computed using the initial grid. Inviscid features are identified and further resolved in the initial flowfield solution using the previously described adaptation sources. Selected streamlines are tracked and grouped as sets of points to resolve detached viscous regions. Using the streamline points and adaptation sources, a new solution-adapted grid is generated. A starting flowfield for the solution-adapted grid is then interpolated from the initial flowfield solution and grid. Starting with this flowfield, a new solution is obtained. This process can be repeated until a desired level of resolution is achieved.

The adaptation source generation as well as the streamline generation, point distribution, and insertion processes are automated so that a viscous solution-adapted grid can be generated in a few minutes on a personal computer or workstation. The efficiency of the standard

Received May 1, 1995; presented as Paper 95-1726 at the AIAA 12th Computational Fluid Dynamics Conference, San Diego, CA, June 19–22, 1995; revision received July 9, 1996; accepted for publication July 14, 1996; also published in *AIAA Journal on Disc*, Volume 2, Number 1.

*Professor, MSU/NSF Engineering Research Center, Department of Mechanical Engineering, P.O. Box 9627. Senior Member AIAA.

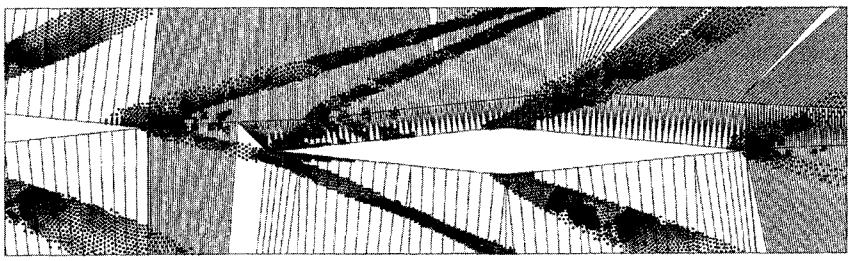

Fig. 1 Triangulation of boundary points including embedded wake boundaries and adaptation sources (shown as dots) for supersonic double strut case.

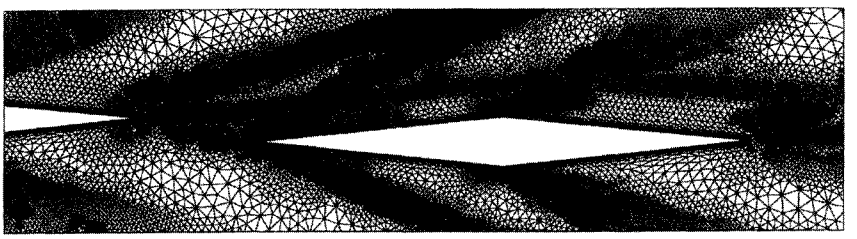

Fig. 2 Second solution-adapted grid for supersonic double strut case.

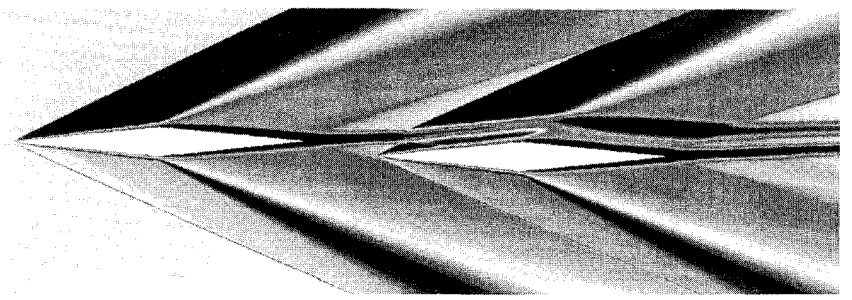

Fig. 3 Computed density contours obtained with second solution-adapted grid for supersonic double strut case.

grid generation procedure is not degraded. For example, CPU time required to generate a solution-adapted grid including wakes with a total of 71,000 points is 20 s on an SGI (Silicon Graphics, Inc.) Indigo-2, R4400-250 Mhz. CPU time required for additional processes, such as adaptation source generation, streamline tracking, and flowfield interpolation, is minimal.

Application Examples

Application examples are presented to demonstrate the overall procedures. The flowfield solutions presented here were obtained using an explicit finite element solver.[9,10] This solver uses a second-order accurate spacial discretization obtained from a Taylor–Galerkin weighted residual approximation. The solution is advanced in time using an explicit two-step Lax–Wendroff scheme.

Supersonic Double Strut

A two-dimensional double strut configuration was considered to demonstrate the capability to capture strong inviscid and viscous features simultaneously. For this case, the freestream Mach number is 3, the angle of attack is 2 deg, and the Reynolds number based on the chord of one strut is 1×10^5. The flowfield was modeled as laminar flow. An initial grid with 5512 points was used to start the solution process. From an initial solution obtained on this grid, two additional adapted grids and solutions were generated. The second solution-adapted grid with 112,126 points is shown in Fig. 2. Regions containing shock waves, strong expansions, and viscous wakes have been refined. Isotropic elements were used for the embedded wake boundaries. Computed density contours for the adapted grid are shown in Fig. 3. Both inviscid and viscous flowfield features are clearly well resolved in the final solution.

Multi-Element Airfoil

A two-dimensional multi-element airfoil case was considered to demonstrate the features of the present viscous solution adaptation procedure with multiple viscous wakes. For this case, the freestream Mach number is 0.2, the angle of attack is 16.2 deg, and the Reynolds number based on chord is 9×10^6. An initial grid with 33,196 points was generated with high-aspect-ratio elements adjacent to boundary surfaces. The initial grid spacing is suitable to capture the boundary-layer and surface pressure distribution. A turbulent flowfield solution was generated using the initial grid.

Using the initial flowfield solution, streamlines were generated from the lower and upper slat trailing edges, the main airfoil trailing edge and lower cove edge, and from the flap trailing edge. An adapted grid for this case with 126,735 grid points was obtained using isotropic wake elements. For comparison, an equivalent adapted grid with 70,949 points was obtained using high-aspect-ratio wake elements. Both of these adapted grids, as well as the initial grid, are shown in Fig. 4. Adaptation sources for inviscid features were not used for this case with either adapted grid as the initial grid provides sufficient resolution.

A final turbulent flowfield solution was generated using the solution-adapted grid. Computed and experimental pressure coefficient distributions (not shown) are in good agreement.[8] This is expected as the surface pressure by itself can be predicted nearly as well with significantly fewer total points. However, resolution of the wake regions requires a high grid point density in the field. Computed Mach number contours for the initial and adapted solution with isotropic wake elements are shown in Fig. 5. Although the initial solution appears reasonable in some areas, the resolution of the wakes is not adequate, especially the slat wake above the flap. The resolution of the wake regions has been improved substantially with the adapted grid. For example, the front slat wake is resolved all of the way past the rear flap. Adaptation has clearly improved the resolution of the wakes. These results demonstrate that adaptation of viscous regions in the field provides substantially improved resolution and can be obtained using a relatively simple procedure.

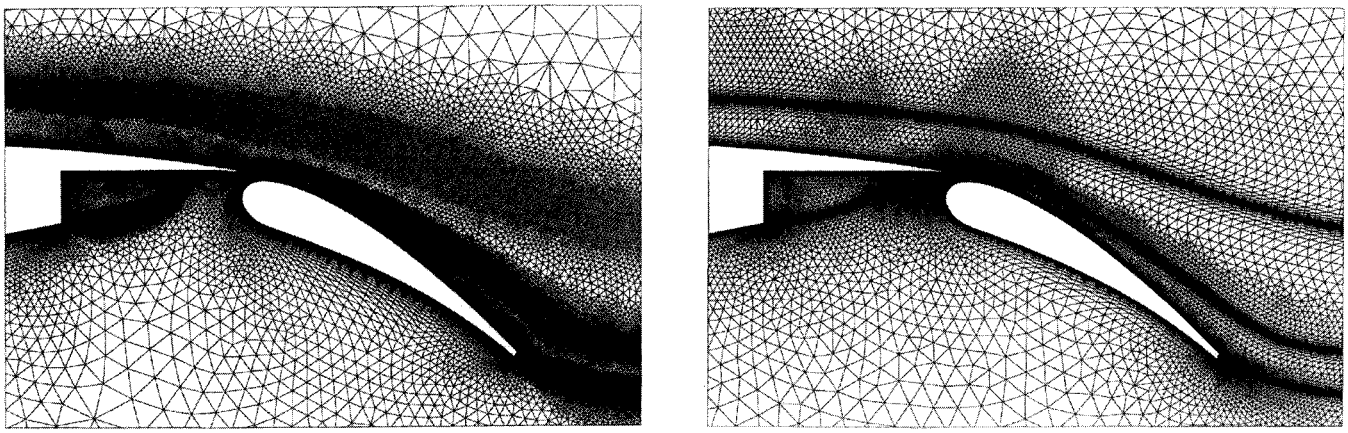

a) Adapted grid with isotropic wake elements near rear flap

b) Adapted grid with high-aspect-ratio wake elements near rear flap

Fig. 4 Detail views of grids for multi-element airfoil case.

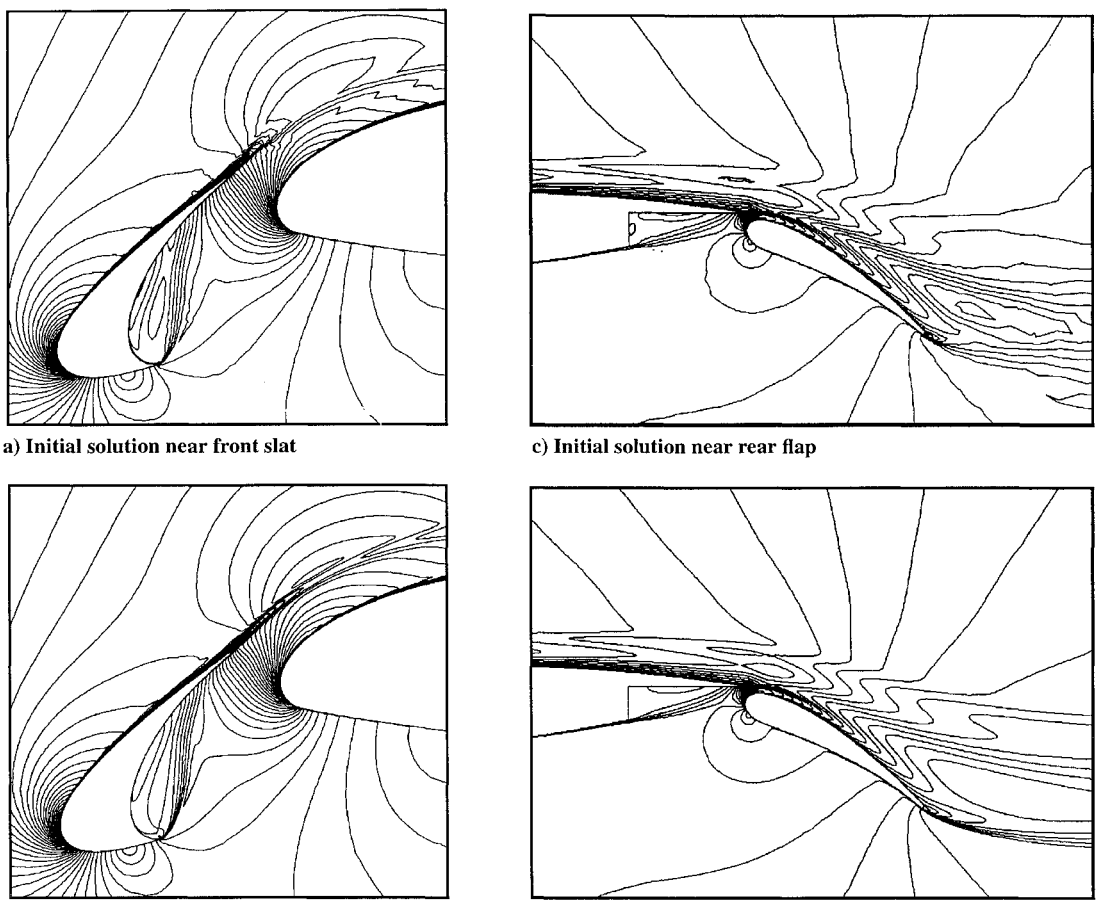

a) Initial solution near front slat

c) Initial solution near rear flap

b) Adapted solution near front slat

d) Adapted solution near rear flap

Fig. 5 Detail views of computed Mach number contours for multi-element airfoil case.

Summary

A procedure has been presented for efficient generation of high-quality solution-adapted grids suitable for viscous flow applications. In this procedure, inviscid type features, such as shock waves and stagnation points, are resolved using adaptation sources derived from the flowfield solution. Detached viscous features, such as wakes, are resolved by tracking selected streamlines and treating them as embedded boundaries. This provides a natural framework for directional refinement and automatic alignment with the wake using advancing-point point placement. Results presented for two-dimensional cases with multiple viscous wakes and strong inviscid features demonstrated that significantly improved resolution of the flowfield can be obtained.

Acknowledgments

The author would like to acknowledge support for this work from the U.S. Air Force Office of Scientific Research, Ford Motor Company, and Boeing Commercial Airplane Company.

References

[1]Hassan, O., Morgan, K., Peraire, J., Probert, E. J., and Thareja, R. R., "Adaptive Unstructured Mesh Methods for Steady Viscous Flow," AIAA Paper 91-1538, June 1991.

[2]Bristeau, M., Mallet, M., Periaux, J., and Roge, G., "Development of Finite Element Methods for Compressible Navier–Stokes Flow Simulations in Aerospace Design," AIAA Paper 90-0403, Jan. 1990.

[3]Holmes, D. G., and Connell, S. D., "Solution of the 2D Navier–Stokes Equations on Unstructured Adaptive Grids," AIAA Paper 89-1932, June 1989.
[4]Kallinderis, Y., and Nakajima, K., "Finite Element Method for Incompressible Viscous Flows with Adaptive Hybrid Grids," *AIAA Journal*, Vol. 32, No. 8, 1994, pp. 1617–1625.
[5]Marcum, D. L., "Generation of Unstructured Grids for Viscous Flow Applications," AIAA Paper 95-0212, Jan. 1995.
[6]Marcum, D. L., and Weatherill, N. P., "Unstructured Grid Generation Using Iterative Point Insertion and Local Reconnection," *AIAA Journal*, Vol. 33, No. 9, 1995, pp. 1619–1625.
[7]Marcum, D. L., and Weatherill, N. P., "A Procedure for Efficient Generation of Solution Adapted Unstructured Grids," *Computer Methods in Applied Mechanics and Engineering*, Vol. 127, 1995, pp. 259–268.
[8]Marcum, D. L., Weatherill, N. P., Marchant, M. J., and Beaven, F., "Adaptive Unstructured Grid Generation for Viscous Flow Applications," AIAA Paper 95-1726, June 1995.
[9]Marcum, D. L., and Agarwal, R. K., "A Finite-Element Flow Solver with $k-\epsilon$ Turbulence Model for Unstructured Grids," *AIAA Journal*, Vol. 30, No. 3, 1992, pp. 648–654.
[10]Marcum, D. L., and Weatherill, N. P., "Turbulence Models for Unstructured Finite Element Calculations," *International Journal for Numerical Methods in Engineering*, Vol. 20, 1995, pp. 803–817.

Improved Jet Coverage Through Vortex Cancellation

B. A. Haven* and M. Kurosaka†
University of Washington, Seattle, Washington 98195-2400

I. Introduction

In film cooling used in gas turbines, coolant from compressors is introduced to the hot gas stream of the turbine as crossflow jets. The jets form a film layer of cooler air that acts to insulate the turbine material from the hot combustion gases. Thus the ability of coolant jets to adhere to the surface is of crucial importance for the effectiveness of film cooling.

The interaction of the coolant jet and crossflow results in the formation of a pair of counter-rotating vortices, or kidney vortices. The sense of rotation of the kidney vortices is such that they exert two undesirable effects (Fig. 1): 1) hot air is forced down beneath the jet to the turbine wall, and 2) the vortices tend to lift the jet off the surface by the mutual induction between the vortex pair. Here we report the potential of promoting jet attachment by weakening the kidney vortices through cancellation. This is accomplished by introducing a vortex pair inside the jet passage that has a sense of rotation opposite to the kidney vortices (Fig. 2). (Even without the installation of vanes, the canceling vortex pair, or negative pair, can also be formed by proper contouring of the hole exit geometry.[1,2])

II. Experiments

A. Experimental Apparatus

The experiments were conducted in the University of Washington water tunnel facility.[1] The tunnel speed was 8 cm/s. At 26.4 cm from the leading edge of the test plate, a jet was injected from a 3.18-cm-diam (d) hole perpendicular to the oncoming crossflow. The displacement thickness of the crossflow boundary layer, which was laminar, was 0.3 cm. Within the jet passage, two vanes were installed at the sides of the hole, 5.3 cm from the exit ($z/d = -1.7$). By placing these vanes at an angle relative to the flow within the jet passage, a distinct counter-rotating vortex pair was generated as shown in Fig. 3.

The general liftoff behavior of the jet is governed by the blowing ratio, BR, which is the ratio of the mass flux of the jet to the mass flux of the crossflow. Since the densities of both the crossflow and jet are the same, the blowing ratio can be written as a ratio of velocities:

$$BR \equiv \rho U_j / \rho U_\infty = U_j / U_\infty \tag{1}$$

The blowing ratio for the results presented is 1.6. At this ratio the jet with no vane deflection is completely detached from the surface. This selection thus enables the influence of the vanes to promote jet attachment to be more easily detected. Laser-induced fluorescence and particle image velocimetry were used to visualize the jet and to quantify the vorticity, respectively (for details, see Haven[1]).

B. Results

The kidney vortices can be traced to the vorticity originating within the jet passage boundary layer. This vorticity is initially aligned circumferentially; that is, there is no z component of vorticity w_z. As shown in Fig. 3b, deflection of the vanes generates a z component of vorticity. As a consequence, within the hole passage the jet boundary-layer vorticity and vane-generated vorticity do not interact with each other. Therefore, for this vane-generated vortex pair to have a canceling effect, the jet vorticity must first be turned.

As the jet exits the hole, the crossflow skews the velocity profile toward the downstream. The jet boundary layer along the sides of the hole is turned upward, which realigns the circumferential

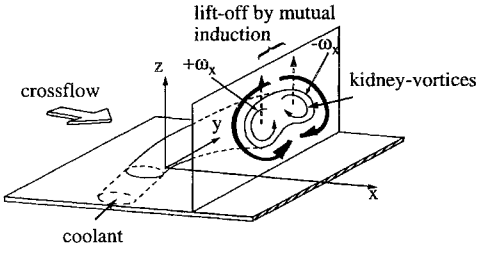

Fig. 1 Kidney vortices represented as $(\omega_x, -\omega_x)$.

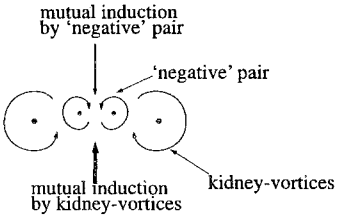

Fig. 2 Vorticity reduction through cancellation.

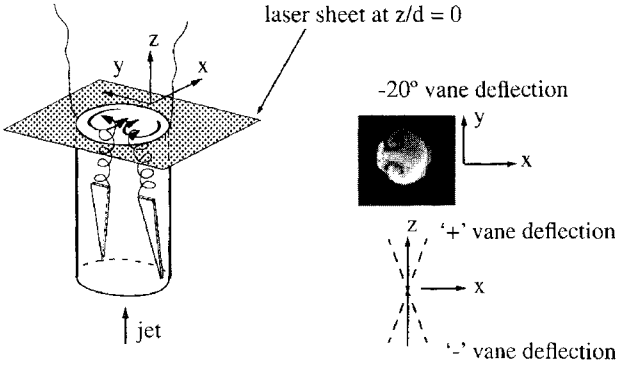

Fig. 3 a) Schematic of vortex pair generation using vanes placed at an angle of attack relative to the jet flow—no crossflow, and b) flow visualization using a laser sheet in the x–y plane located at the plate surface, $z/d = 0$. Vane deflection is −20 deg.

Received May 17, 1996; revision received July 3, 1996; accepted for publication Aug. 6, 1996; also published in *AIAA Journal on Disc*, Volume 2, Number 1. This paper is declared a work of the U.S. Government and is not subject to copyright protection in the United States.

*Graduate Student, Department of Aeronautics and Astronautics; currently Assistant Professor, Department of Aeronautics, U.S. Air Force Academy, HQ USAFA/DFAN, 2354 Fairchild Drive, Suite 6H22, Colorado Springs, CO 80840-6222. Member AIAA.
†Professor, Department of Aeronautics and Astronautics, Box 352400. Associate Fellow AIAA.